Thermal expanded core ultraviolet fiber for optical cavity mode matching

Xin-Xia Gao (高新霞)[1,2], Jin-Ming Cui (崔金明)[1,2,*], Yun-Feng Huang (黄运锋)[1,2], Chuan-Feng Li (李传锋)[1,2], and Guang-Can Guo (郭光灿)[1,2]

[1]*CAS Key Laboratory of Quantum Information, University of Science and Technology of China, Hefei 230026, China*

[2]*CAS Center for Excellence in Quantum Information and Quantum Physics, University of Science and Technology of China, Hefei 230026, China*

**Corresponding author: jmcui@ustc.edu.cn*

Received February 15, 2019; accepted May 17, 2019; posted online July 23, 2019

We have demonstrated a mode matching method between two different fibers by a hybrid thermal expanded core technique, which can be applied to match the modes of fiber-based Fabry–Pérot cavities. Experimentally, this method has achieved an expansion of the ultraviolet fiber core by 3.5 times while keeping fundamental mode propagation. With the experiment parameters, the fundamental mode coupling efficiency between the fiber and micro-cavity can reach 95% for a plano-concave cavity with a length of 400 μm. This method can not only have potential in quantum photonics research but also can be applied in classical optical fields.

OCIS codes: 060.2310, 120.2230, 140.3948, 020.5580.

doi: 10.3788/COL201917.090601.

Fiber-based Fabry–Pérot cavities (FFPCs) are widely used in many applications[1,2], benefitting from their high finesse and small volume in recent years. However, mode matching between the cavity mode and input/output fibers modes has been the main hindrance for many applications. Especially in research fields with trapped ions, due to the strong disturbance of the trapping electric potential by the presence of the dielectric fibers, trapping of ions in the close vicinity of a fiber mirror is challenging. Hence, relatively long cavities are desirable. However, a long cavity leads to a large cavity mode. On the other hand, the trapped ions radiate fluorescence in the ultraviolet range; to enhance the fluorescence of trapped ions with an FFPC, ultraviolet fibers with a small fiber core are used to fabricate the FFPC. As a result, the mode mismatching between fibers and cavities will decrease the coupling efficiency. To improve it, large mode single-mode fibers (SMFs) are greatly essential. Many efforts have been done, such as the application of a photonic crystal fiber[3,4] and the splicing of different types of fibers for a fiber assembly[5]. These methods use special fibers that are extremely fragile and sensitive to the external environment or need very strict operation skills with low reproducible ability.

In this Letter, we demonstrate a hybrid thermal expanded core (TEC) method with two kinds of fibers that can be used to match the optical modes between the FFPC micro-cavity and fiber. The TEC technique can reduce the index difference between the fiber core and cladding by heating the fibers to expand the mode field diameter (MFD). It has been developed for decades, which is an important technique in the fields of optical communication and optical sensing, for example, in the reduction of splice losses between different types of fibers, such as erbium-doped fibers to standard SMFs[6–9], and the design of lens-free devices[10–12]. In fact, there are two kinds of fibers[9]: one is a germanium-doped core and pure-silica cladding; another is designed with an un-doped, pure-silica core surrounded by a depressed, fluorine-doped cladding, which is designed to reduce photo-darkening. The fluorine-doped cladding fiber is ideal for fluorescence spectroscopy and other applications at short visible or ultraviolet wavelengths. In the past, the core expansion work was carried out just for germanium-doped ions. For fluorine-doped fibers, we demonstrate a new method to achieve the appropriate multiple expansion by employing two kinds of SMFs. As the core expansion region can be recognized as an adiabatic region, the mode coupling efficiency from the original fiber core to the expanded core is almost 100%. The TEC technique can be applied to almost any kind of SMF for better mode matching, making this approach highly versatile and practical for many applications.

For fluorine-doped fibers, the theoretical calculation of refractive index distribution is the same as the analysis of the germanium-doped fibers[13–15]. As the expanded region is long enough, it is reasonable to ignore the diffusion in the longitude. Note the dopant concentration for the cross section of the TEC fiber as $u(r,t)$, which is a function of the radial distance r and heating time t. The diffusion function of the doped fluorine ions in cylindrical coordinates can be written as follows:

$$D\frac{\partial^2 u}{\partial r^2}+\frac{D}{r}\frac{\partial u}{\partial r}=\frac{\partial u}{\partial t}, \tag{1}$$

where D is the diffusion coefficient of the dopant, which can be expressed as

$$D = D_0 \exp\left(-\frac{Q}{RT}\right), \tag{2}$$

where $D_0 = 9 \times 10^{-6}\ \mathrm{m^2/s}$ is the constant factor of vibration, and Q is the activation energy of ions; for fluorine ions, Q is 3.83×10^5 J/mol. T is the thermodynamic temperature, and $R = 8.31$ J/(K · mol) is the gas constant. Thus, D is a function of temperature[16,17]. Assume that the initial dopant concentration is in the form of δ function; through numerical solving, we obtain the concentration distribution of the doped fluorine ions.

The refractive index of TEC fiber is determined by the density of fluorine dopant, which can be given by[18]

$$n^2(r) = n_1^2 + (n_0^2 - n_1^2)u(r,t), \tag{3}$$

where n_0 and n_1 are the original refractive index of the core and clad, respectively. As a result, we can get the refractive index distribution after heating at different times. The distribution curves are shown in Fig. 1; as the heating time increases, the refractive index of the core decreases, and the effective core radius increases.

Next, we use finite element method software (COMSOL) to simulate the fundamental eigenmode in different expanded cores. By importing the simulated refractive index data in Fig. 1 into COMSOL, setting the frequency to 8.11×10^{14} Hz, and searching for modes around 1.46, we then get the mode analysis result. Figure 2 shows different fundamental modes corresponding to different periods of time: $T = 0$, $T = 5$ min, $T = 15$ min, and $T = 40$ min, and the MFD keeps growing and always maintains the single-mode (SM) transmission.

There are several methods to heat the fiber, such as hydrogen/oxygen flame, CO_2 laser, electric furnace, and fiber fusion splicer[19–21]. Flame heating is a relatively traditional and mature method. Hydrogen/oxygen is an improved flame, which will not cause air pollution. The CO_2 laser can effectively reduce the time to fabricate the TEC fiber, but it is difficult to modulate the laser parameters for effective heating. An electric furnace is suitable for a mass process with an obvious defect for more than 40 h of heating time. Here, we use the hydrogen/oxygen flame as a heat source, as shown in Fig. 3, where an SM300 (Thorlabs, fluorine-doped) fiber with an initial MFD of 2.2 μm is clamped on a fiber mount, and the cleaved end facet of the fiber is heated by outer flame. A laser beam profiler (Newport LBP2) was used to measure the spot size.

When the radiation propagating in an SMF reaches a cleaved end-face, it radiates from the fiber to the surrounding air. The light diffracts as it leaves the fiber, and the resulting electromagnetic field evolves from a near-field distribution close to the fiber end-face into a far-field distribution further away. It behaves like a Gaussian beam in free-space with the beam waist at the end-face of the TEC fiber[6]. Therefore, when the

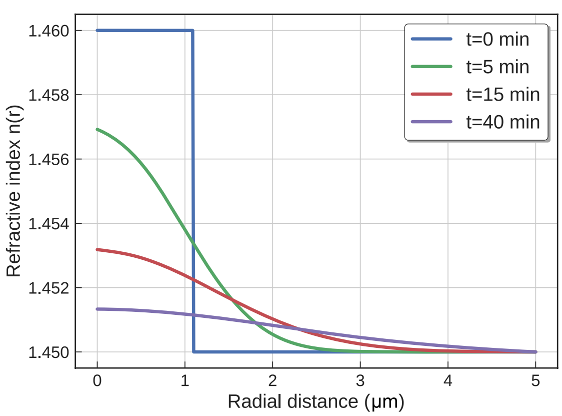

Fig. 1. Simulation of refractive index distribution versus radial distance from the fiber core with different thermal expanding times.

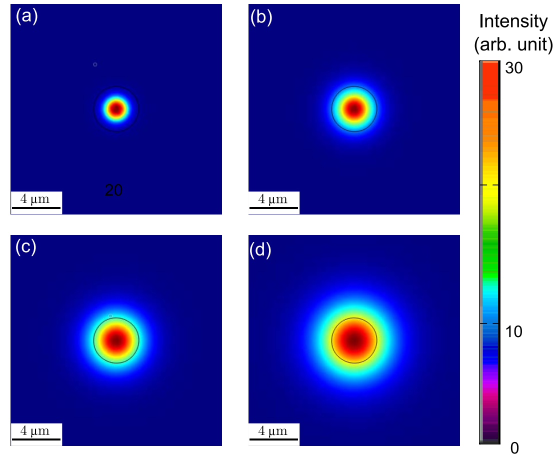

Fig. 2. Diagram of fiber mode simulation by the finite element method. Fundamental mode with heating time at (a) $T = 0$ min, (b) $T = 5$ min, (c) $T = 15$ min, (d) $T = 40$ min, respectively. Comparing (d) to (a), the spot is increased by about seven times, and the Gaussian pattern shows that the fundamental mode propagating in the TEC fiber is maintained.

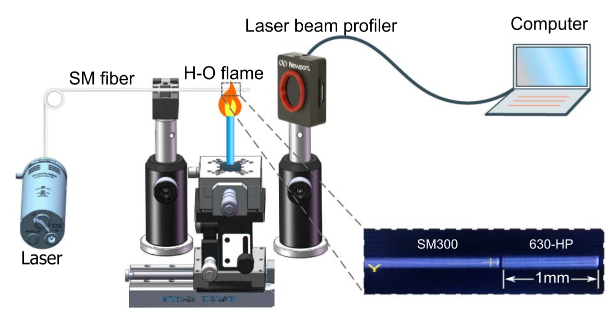

Fig. 3. Setup diagram of fiber core expansion. An SMF is held on the fiber mount and heated by a hydrogen/oxygen flame, and the beam profiler is used to monitor the spot size to determine the divergence of the beam after the TEC fiber, which finally indicates the MFD of the TEC fiber. The magnified inset is a photo of the target fiber in a fiber fusion splicer. It is a combination of an SM300 fiber and 630-HP fiber, where the length of the 630-HP fiber is controlled within 1 mm, and the heating region is focused on the splicing.

propagation length z is much larger than Rayleigh length z_R, the radius of the beam $w(z)$ increases linearly with z according to the Fraunhofer approximation in the far-field condition, and the half-divergence of the beam is given by

$$\theta \simeq \frac{2\lambda}{\pi\omega_0}, \tag{4}$$

where ω_0 is the radius of the beam waist, which is half of the MFD. Equation (4) shows that the half-divergence θ is inversely proportional to the radius of the beam waist ω_0 under far-field conditions. Therefore, for a given wavelength λ, we can obtain the MFD's variation by the beam divergence's variation. The laser beam profiler is set at a certain distance d from the end of the fiber, and we can read the radius of the Gaussian spot $\omega(z)$, where the intensity has dropped to $1/e^2$ of its on-axis value. Then, the half-divergence θ can be given by

$$\theta \simeq \frac{\omega(z)}{d}. \tag{5}$$

So, the half-divergence has been converted to record the radius of the Gaussian spot $\omega(z)$.

We have tested expanding an SM300 fiber directly in this case; the SM300 fiber is a fluorine-doped fiber, which is used to collect 369 nm fluorescence from the Yb^+ ion, and the SM300 fiber can be enlarged by two times at most when maintaining the fundamental Gaussian mode. In past work, the germanium-doped fiber can be expanded 3.3 times[22]. There are two possible reasons to explain it: one is the instability of the doped fluorine ions, and the other is the effect of stress occurring when the fire is removed.

To further enlarge the field mode diameter of the ultraviolet fiber, we splice another SMF with a larger MFD. We choose an SMF of 630-HP (Nufern, germanium-doped), as its MFD is about 4 μm, which is as large as the SM300 fiber after TEC treatment. It makes it probable to couple with each other with higher efficiency. Before heating, the 630-HP is spliced to a cleaved SM300. Then, the spliced fiber is cleaved again by leaving 1 mm length of the 630-HP fiber. The transmission loss of 630-HP at 369 nm is measured as 0.26 dB/cm, so the transmission of the 1 mm 630-HP fiber is 99.4%. At first, there is a lot of laser light leaking out at the splicing due to the quite different MFD. Then, we put the spliced fiber on the outer flame and move the position of the fiber to make sure that the splicing point can be heated sufficiently. During this heating process, the light leakage at the splicing point will darken, which means that the two modes are coupled more efficiently. This interesting phenomenon can be explained in this way: as the spliced fiber is heated, fluorine ions in SM300 fiber and germanium ions in the 630-HP fiber are diffused. Due to activation energy of fluorine ions being higher than that of germanium ions, the MFD of the SM300 fiber can be expanded much more quickly than that of the 630-HP fiber. Finally they tend to be the same size after about 5 min heating.

The various spot changes during the whole process are recorded from the profiler in Fig. 4 every 45 s. Initially, a considerable part of the laser leaks to the cladding of the fiber. As both of the fiber cladding and fiber core support multi-transverse modes of the laser, different modes interfere to form interference fringes in Fig. 4(b). With the TEC processing, the MFD gets closer between the two fibers, more of the laser beam is coupled into the core, the interference fringes gradually shrink, and the central area gets brighter and brighter at the same time. After about 5 min, more than 95% of the laser beam was coupled into the fundamental mode, and the spot became a Gaussian spot. Comparing the final picture with the initial one, the radius of the Gaussian spot $\omega(z)$ is 2.6 and 0.74 mm, respectively. As the beam propagation distance $d = 22.5$ mm, half-divergence θ decreases by about 3.5 times; on the other hand, the MFD of the TEC fiber is expanded by 3.5 times.

After TEC treatment, the end facet of the TEC fiber can be structured as a concave surface by the CO_2 laser pulse and coated with a highly reflective dielectric coating[23]. Then, they can be employed to set up an FFPC, which can be in one of two configurations, as shown in Fig. 5, the symmetric concave cavity or the plano-concave cavity. As the cavity mirrors are part of the in-coupling and out-coupling fibers, the coupling efficiency is given directly by the mode matching between the fiber mode and the cavity mode. Considering symmetric cavities for simplicity, the mode radius on the cavity mirrors is

$$\omega_m = \sqrt{\omega_c^2 + \frac{\lambda L}{2\pi}}, \tag{6}$$

where $\omega_c = \sqrt{\frac{\lambda}{2\pi}}[L(2R-L)]^{\frac{1}{4}}$ is the waist radius of the cavity mode, R is the radius of curvature (ROC) of the

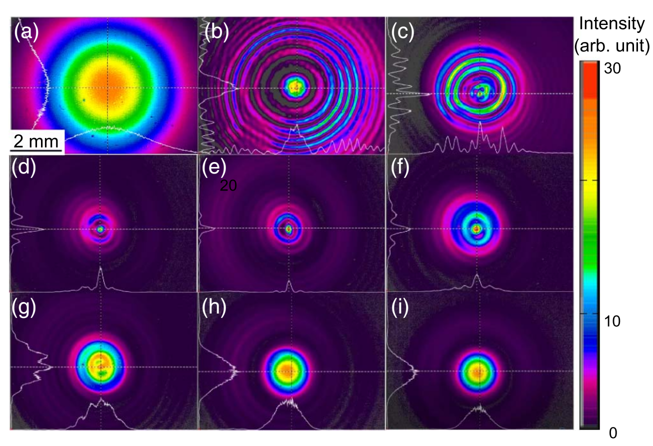

Fig. 4. Spot changes when heating the splicing between the SM300 fiber and 630-HP fiber. (a) The initial SM300 with half-divergence $\theta = 0.116$ rad; (b)–(h) the spot change process; (i) the final Gaussian spot with half-divergence $\theta = 0.033$ rad. The 3.5-fold reduction in half-divergence is equivalent to a 3.5-fold increase in the MFD of the TEC fiber.

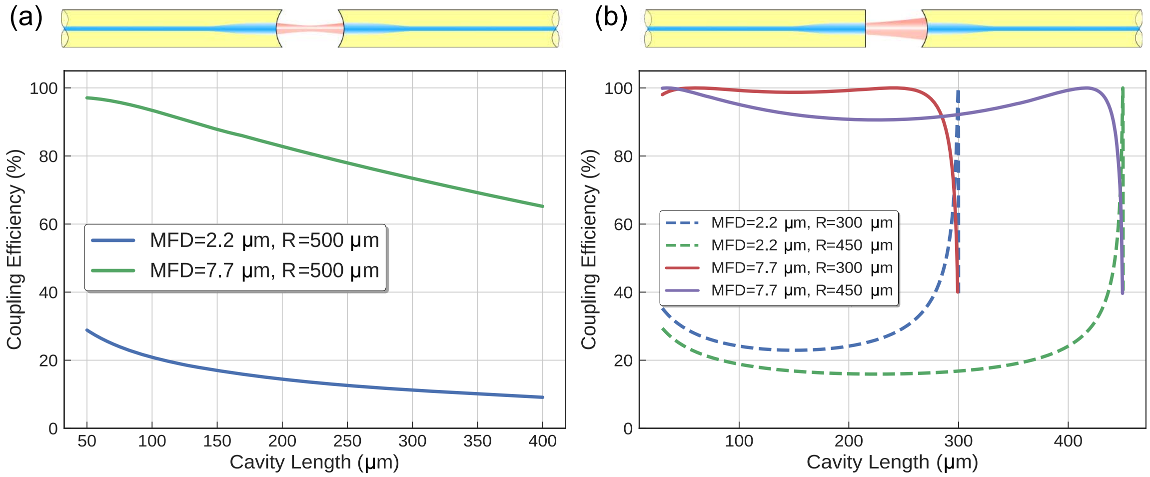

Fig. 5. (a) Mode matching efficiency between fiber and cavity mode for a symmetric concave cavity. The blue line shows the initial SM300 fiber for the FFPC, where the coupling efficiency is about 30% at the cavity length of 50 μm. The green line is the result after TEC treating; the efficiency can achieve 75% when the cavity length is 300 μm. (b) Mode matching between the fiber and cavity mode for a plano-concave cavity. Considering the flat end coupling with the cavity mode, as the dotted line shows, the initial fiber can form a stable cavity with coupling efficiency around 20%; when the MFD comes to 7.7 μm, the coupling efficiency can always be above 90%, as the solid line shows. The purple line shows that the coupling efficiency can be more than 95% with a large cavity length of around 400 μm.

mirrors, and L is the cavity length. For an SM fiber with its nearly Gaussian transverse mode profile of radius $\omega_f = \mathrm{MFD}/2$, and assuming that the cavity mode is well aligned with the fiber axis, the fiber-to-cavity power coupling efficiency can be approximated by the mode overlap of two Gaussian modes[24,25]:

$$\epsilon = \frac{4}{\left(\frac{\omega_m}{\omega_f} + \frac{\omega_f}{\omega_m}\right)^2 + \left(\frac{\pi n_f \omega_f \omega_m}{\lambda R}\right)^2}, \tag{7}$$

where n_f is the refractive index of the SM fiber. From this expression, we know that the optimum coupling occurs around $\omega_m = \omega_f$. However, to assemble with an ion trap setup, the required cavity length usually is more than 200 μm, which is to minimize trap distortion due to the charging effect on the dielectric coating of the cavity. As L is increased, the mode radius on the mirrors ω_m will also increase. Especially, the ultraviolet fiber has an extraordinarily small mode radius ω_f. Therefore, an expanded core SMF is necessary.

Using Eq. (7), we calculate the optimal coupling efficiency between the fiber and cavity mode. The result of the symmetric concave cavity is shown in Fig. 5(a); the initial SM300's MFD is 2.2 μm, and when the cavity length is more than 50 μm, the efficiency drops below 30%. After expanding, the expanded MFD is 7.7 μm, and the efficiency can be above 75% even if the cavity length is 300 μm.

Considering plano-concave mirrors for cavity configuration, and using the flat end to collect photons, it can match better because the beam waist of the laser beam is on the end of the fiber. The calculation of mode matching between the SMF and a flat-concave cavity is displayed in Fig. 5(b), where the initial SMF can form a stable cavity with coupling efficiency around 20%; for the expanded core fiber, the coupling efficiency can always be above 90%, as the solid line shows. The solid purple line shows that when the ROC is machined to 450 μm, the coupling efficiency can be more than 95% with the large cavity length around 400 μm.

We have demonstrated a method to apply the TEC technique to an ultraviolet fiber. The direct TEC treatment can just expand the fluorine-doped fiber core by two times, probably because of the more active fluorine ions. It can be solved by splicing the 630-HP fiber to the SM300 fiber and heating the splicing for about 5 min. Then, the two parts can be coupled with each other perfectly, finally getting the 3.5 times expanding effect and keeping good fundamental characteristics.

The ultraviolet TEC fiber can be fabricated to FFPCs with large cavity length, which solves the main limitation of mode matching between the fiber and cavity mode in ultraviolet FFPCs integrated into a Yb^+ ion trap. For the symmetric concave cavity, it can achieve a mode matching of 75% for a cavity length of 300 μm, and for the plano-concave cavity, the coupling efficiency can be about 95% for a cavity length around 400 μm.

We acknowledge funding support from the National Key Research and Development Program of China (Nos. 2017YFA0304100, 2016YFA0302700), the National Natural Science Foundation of China (Nos. 11774335, 11474268, 11734015, 11821404), Key Research Program of Frontier Sciences, CAS (No. QYZDY-SSW-SLH003), the Fundamental Research Funds for the Central Universities (Nos. WK2470000026, WK2470000018), Anhui Initiative in Quantum Information Technologies (Nos. AHY020100, AHY070000).

References

1. T. Ballance, H. Meyer, P. Kobel, K. Ott, J. Reichel, and M. Köhl, Phys. Rev. A **95**, 033812 (2017).
2. E. Kassa, H. Takahashi, C. Christoforou, and M. Keller, J. Mod. Opt. **65**, 520 (2018).
3. T. Popplau, K. Ott, S. Garcia, F. Ferri, R. Kohlhaas, K. Schüppert, R. Long, and J. Reichel, in *APS Division of Atomic, Molecular and Optical Physics Meeting* (2017).
4. J. Villatoro, V. Finazzi, G. Coviello, and V. Pruneri, Opt. Lett. **34**, 2441 (2009).
5. G. K. Gulati, H. Takahashi, N. Podoliak, P. Horak, and M. Keller, Sci. Rep. **7**, 5556 (2017).
6. G. Kliros and N. Tsironikos, Optik **116**, 365 (2005).
7. C. Kopp and L. Fulbert, Opt. Commun. **235**, 175 (2004).
8. M.-C. Oh, S.-H. Cho, and H.-J. Lee, Opt. Commun. **246**, 337 (2005).
9. K. Shiraishi, Y. Aizawa, and S. Kawakami, J. Lightwave Technol. **8**, 1151 (1990).
10. T. Sato, R. Kasahara, J. Sun, and S. Kawakami, IEEE Photon. Technol. Lett. **9**, 943 (1997).
11. R. Syms, H. Zou, J. Stagg, and H. Veladi, J. Micromech. Microeng. **14**, 1700 (2004).
12. W. Zheng, O. Hulten, and R. Rylander, J. Lightwave Technol. **12**, 430 (1994).
13. F. Dong, X. Zhang, and F. Song, Chin. Opt. Lett. **16**, 030602 (2018).
14. M. Kihara, M. Matsumoto, T. Haibara, and S. Tomita, J. Lightwave Technol. **14**, 2209 (1996).
15. X. Zhou, Z. Chen, H. Chen, J. Li, and J. Hou, Opt. Laser Technol. **47**, 72 (2013).
16. S. Savovic and A. Djordjevich, Opt. Mater. **30**, 1427 (2008).
17. J. Kirchhof, S. Unger, K.-F. Klein, and B. Knappe, J. Non-Cryst. Solids **181**, 266 (1995).
18. Y. Ohtera, O. Hanaizumi, and S. Kawakami, J. Lightwave Technol. **17**, 2675 (1999).
19. S.-J. Kim and J.-M. Kim, US Patent 6,244,757 (2001).
20. K. Inoue, K. Sasaki, Y. Suzuki, N. Kawanishi, and Y. Tsutsumi, US Patent 6,294,760 (2001).
21. G. Rego, O. Okhotnikov, E. Dianov, and V. Sulimov, J. Lightwave. Technol. **19**, 1574 (2001).
22. O. Hanaizumi, Y. Aizawa, H. Minamide, and S. Kawakami, IEEE Photon. Technol. Lett. **6**, 842 (1994).
23. H. Takahashi, J. Morphew, F. Oručević, A. Noguchi, E. Kassa, and M. Keller, Opt. Express **22**, 31317 (2014).
24. D. Hunger, T. Steinmetz, Y. Colombe, C. Deutsch, T. W. Hänsch, and J. Reichel, New J. Phys. **12**, 065038 (2010).
25. K. Shiraishi, T. Yanagi, and S. Kawakami, J. Lightwave Technol. **11**, 1584 (1993).